2017

CHARGE TRANSPORT IN ELECTRONIC-IONIC COMPOSITES

Long Zhang
University of Kentucky, long.zhang@uky.edu
Digital Object Identifier: https://doi.org/10.13023/ETD.2017.427

STUDENT AGREEMENT:

I represent that my thesis or dissertation and abstract are my original work. Proper attribution has been given to all outside sources. I understand that I am solely responsible for obtaining any needed copyright permissions. I have obtained needed written permission statement(s) from the owner(s) of each third-party copyrighted matter to be included in my work, allowing electronic distribution (if such use is not permitted by the fair use doctrine) which will be submitted to UKnowledge as Additional File.

I hereby grant to The University of Kentucky and its agents the irrevocable, non-exclusive, and royalty-free license to archive and make accessible my work in whole or in part in all forms of media, now or hereafter known. I agree that the document mentioned above may be made available immediately for worldwide access unless an embargo applies.

I retain all other ownership rights to the copyright of my work. I also retain the right to use in future works (such as articles or books) all or part of my work. I understand that I am free to register the copyright to my work.

REVIEW, APPROVAL AND ACCEPTANCE

The document mentioned above has been reviewed and accepted by the student's advisor, on behalf of the advisory committee, and by the Director of Graduate Studies (DGS), on behalf of the program; we verify that this is the final, approved version of the student's thesis including all changes required by the advisory committee. The undersigned agree to abide by the statements above.

Long Zhang, Student

Dr. Yang-Tse Cheng, Major Professor

Dr. Matthew J. Beck, Director of Graduate Studies

CHARGE TRANSPORT IN ELECTRONIC-IONIC COMPOSITES

THESIS

A thesis submitted in partial fulfillment of the
requirements for the degree of Master of Science in Materials Science and Engineering
in the College of Engineering
at the University of Kentucky

By
Long Zhang
Lexington, Kentucky
Director: Dr. Yang-Tse Cheng, Professor of Materials Science
Lexington, Kentucky
2017

ABSTRACT OF THESIS

CHARGE TRANSPORT IN ELECTRONIC-IONIC COMPOSITES

The goal of this thesis is to generate fundamental understandings of charge transport behaviors of composites consisting of garnet structured Al substituted $Li_7La_3Zr_2O_{12}$ (LLZO) electrolyte and $LiCoO_2$ electrode. In order to take full advantage of all-solid-state batteries, bulk type composite electrodes should be introduced to increase energy and power density. However, the charge utilization of bulk type composite electrodes is quite low. Understanding ionic conduction behavior is, therefore, important for improving the performance of all-solid-state batteries, because ion conduction within solids depends on effective pathways. Electronic conductivity can be easily compensated by adding carbon black, but ionic conductivity can only depend on composites electrode itself. Here, we show that electronic and ionic conductivities of composites consisting of $LiCoO_2$ and Al doped LLZO can be achieved separately. 3D reconstructed image obtained from focused ion beam-scanning electron microscope (FIB-SEM) demonstrates that porosity, percolation, and grain boundaries often play antagonistic roles in controlling the charge transport behaviors in the composite electrodes, resulting in an overall conductivity dominated by electrons. This work suggests an approach to optimize electronic and ionic conductivities for bulk type composite electrodes, which may eventually be utilized in all-solid-state batteries.

KEYWORDS: solid electrolyte, composites, charge transport, conductivity, percolation

Author's signature: Long Zhang

Date: November 02, 2017

CHARGE TRANSPORT IN ELECTRONIC-IONIC COMPOSITES

By

Long Zhang

Dr. Yang-Tse Cheng

Director of Thesis

Dr. Matthew J. Beck

Director of Graduate Studies

November 02, 2017

Dedicated to my family

Table of Contents

List of Figures

Chapter 1 Introduction

Liquid electrolyte based lithium ion batteries (LIBs) have, in the past decades, been comprehensively used as power sources for portable electronic devices due to their high energy and power density. However, liquid electrolytes can cause leakage, fire, and explosion of LIBs. Replacing flammable organic liquid electrolytes with nonflammable inorganic solids is highly desirable because it holds the promise of significantly improving safety, offering higher volumetric and gravimetric energy densities, and potentially lowering the cost of batteries by increasing battery life, decreasing dead space, and simplifying battery packaging. The solid electrolyte is the most critical component in solid-state batteries.[1-8] In recent years, there have been extensive efforts in finding solid materials with high lithium-ion conductivities. As a result, a number of promising compounds with significantly high lithium-ion conductivities comparable to that of liquid electrolytes have been introduced. For example, a new lithium super ionic conductor $Li_{10}GeP_2S_{12}$ (LGPS) phase, which was first reported in 2011, reached a relatively high ionic conductivity up to 1.2×10^{-2} S/cm.[9] In 2017, lithium amide-borohydride $Li(BH_4)_{1/3}(NH_2)_{2/3}$ is reported that ionic conductivity can reach up to 6.4×10^{-3} S/cm at 40℃.[10] In the garnet family of $Li_7La_3Zr_2O_{12}$ (LLZO), Ga and Sc doped $Li_{6.65}Ga_{0.15}La_3Zr_{1.90}Sc_{0.10}O_{12}$ exhibits the highest ionic conductivity of 1.8×10^{-3} S/cm at room temperature.[11] In particular, LLZO has recently been widely studied because, unlike $Li_{1.3}Al_{0.3}Ti_{1.7}(PO_4)_3$ (LATP, NASICON) and $Li_{3x}La_{2/3-x}TiO_3$ (LLTO, perovskite), LLZO has both high ionic conductivity and chemical stability against Li metal.

Despite significant improvements, challenges remain in developing practical solid-state batteries. Composite electrodes consisting of cathode particles and an ion-conducting phase can, in theory, overcome the problem of limited electrode

accessibility in high-energy all-solid-state lithium batteries. The solid electrolyte, unlike liquids, cannot penetrate through the pores inside the porous cathode. The limited contact area between the cathode and the solid electrolyte thus reduces the accessibility of ions to the active sites in the cathode, resulting in low utilization of the electrode material. To enhance the ion accessibility of the cathode in high-energy all-solid-state batteries, the number of studies of bulk-type compact composite electrodes has significantly increased in the past few years. The composite electrodes are often a mixture of the cathode (typically an electron conducting phase), conductive carbon (if cathode phase is not highly conductive), and the electrolyte (i.e., an ion conducting phase).[12-15] The composite microstructure is expected to provide sufficient electron and ion transport, however, the design principles of these electronic-ionic composites are largely unknown and need to be determined.

In this thesis, we discuss the microstructure-conductivity relationship in an electronic-ionic composite with a focus on lithium ion conductivity. This study is the first step toward further understanding of conduction behavior of electronic-ionic composites and electrochemical reactions in all-solid multiphase systems.

Chapter 2 Experimental Section

2.1 Synthesis of Al doped LLZO

Al doped LLZO was synthesized by conventional solid-state process using lithium carbonate (purum, ≥99%, SIGMA-Aldrich), lanthanum (III) hydroxide (99.95% trace rare earth metals basis, BEATOWN CHEMICAL), zirconium(IV) oxide (99% trace metals basis, SIGMA- Aldrich) and aluminum oxide (99.5% trace metals basis, SIGMA- Aldrich) as raw materials. The molar ratio of Li, La, Zr and Al is 7.2:3:2:0.3. Extra 3% Li was added to compensate Li loss during calcination and sintering process. The precursors were mixed and calcined in an alumina crucible at 800 °C for 12 h to get rid of residual moisture. The mixture was ball milled in a zirconia jar at 300 rpm for 12 h, and the acetone was removed overnight at 70 °C. Subsequently, the powder was pressed into pellets via cold uniaxial press following calcination at 1000 °C for 12 h. The powder mixture was reground at 300 rpm for 12 h then were dried at 70 °C. Finally, powders were isostatically pressed into pellets. The pressed pellet was then buried in scarifying powder and sintered at 1100 °C for 12 h.

2.2 Preparation of conductivity measurement samples

$LiCoO_2$ (obtained from MTI Cooperation) and as prepared Al doped LLZO were individually milled to fine particles and were then mixed with different weight ratios (1:3, 1:1 and 3:1). Mixed powders were pressed into pellets via uniaxial press, holding at 250 °C for 1 h. The pellets were then sintered at 700 °C for 6 h to enhance the connection between the particles. After heating treatment, the pellets were dry polished to remove the surface impurities.

2.3 Measurements

The microstructure of the materials was characterized by X-ray diffraction (XRD, D500, Siemens, Germany) with copper Kα radiation. FIB-SEM measurement was carried out on a Helios Nanolab 660 (FEI). Reconstruction of 3D FIB-SEM image was finished by using software Avizo.

Two types of configurations were employed to derive the transport properties. For the measurements with blocking electrodes, a gold layer was applied to both sides of the pellet, Pt foils and wires were attached as current collectors. AC impedance measurements were obtained on dense pellets using impedance analyzer (Solartron 1260), at a frequency range of 10^7-1 Hz at AC amplitude of 50 mV. DC tests were established on digital sourcemeter (KEITHLEY 2400). For measuring ionic conductivity, DC test using electron-blocking cell LiAl/LiI/composite/LiI/LiAl was employed. LiI (99%, Sigma Aldrich) and LiAl alloy (Sigma Aldrich) are served as electron-blocking layer and current collector, respectively. The contact resistance was minimized by heat treatment at 200 °C for 20 h inside glovebox antechamber under vacuum.

Chapter 3 Discussions

Fig. 1 shows the X-ray diffraction (XRD) patterns of $LiCoO_2$ and Al-LLZO powders. The measurement conditions were at room temperature, a wavelength of 1.540562 Å, and a 2θ step-size of 0.02 ° from 10 ° to 60 °. The patterns and lattice parameters match well with the $LiCoO_2$ (PDF#50-0653) and cubic garnet phase $Li_5La_3Nb_2O_{12}$ (PDF#45-0109). XRD patterns were analyzed using a full pattern fitting technique using the General Structure Analysis System (GSAS) with the EXPGUI interface.[16-17] For refinement result, $\chi 2=3.04$, wRp=0.16, and Rp=0.12. Lattice parameter of Al-LLZO is calculated to be 12.964 Å, which is close to the reported values from other literature reports.[18-19]

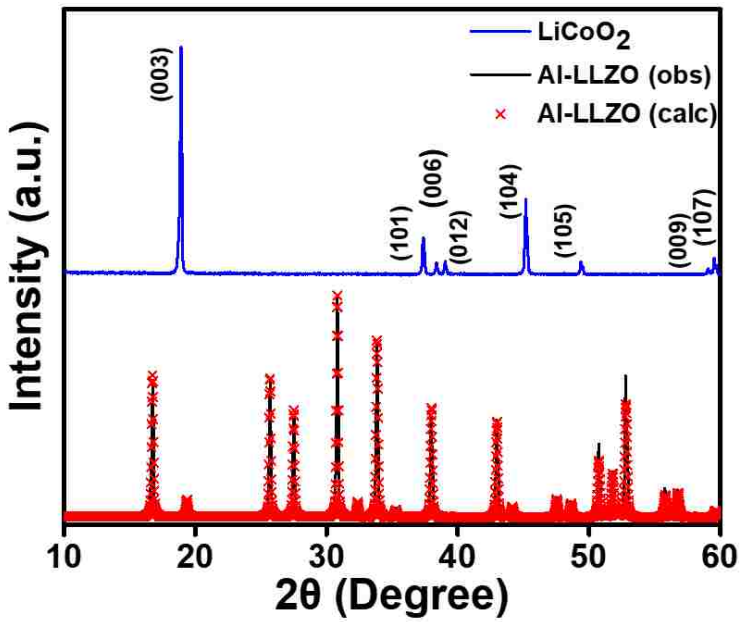

Fig. 1. XRD patterns of (a) $LiCoO_2$, and (b) Al doped LLZO powders.

Cluster size distributions of $LiCoO_2$ and Al-LLZO are presented in Fig.2. We use the term cluster size distribution here, since it is difficult to confirm if in our SEM images we see single particles or agglomerates of smaller particles. The average cluster

sizes are approximately 2.91 μm and 2.53 μm for $LiCoO_2$ and Al-LLZO, respectively. These values show that the two phases before mixing and preparation of composite samples exhibit similar size distributions, and $LiCoO_2$ clusters are slightly larger.

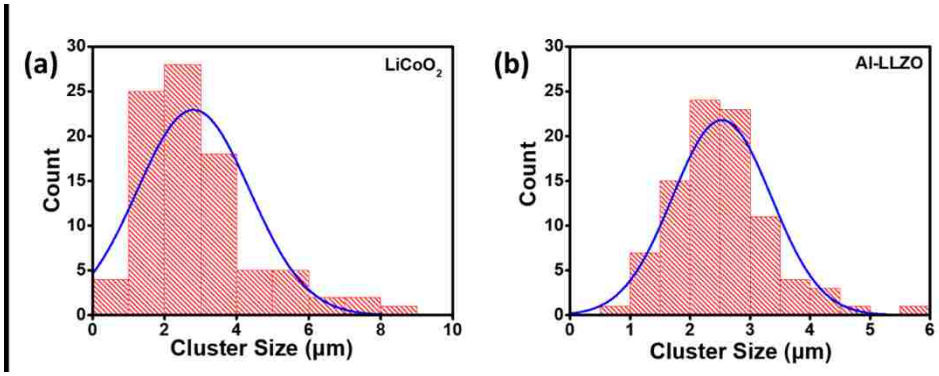

Fig. 2. Size distributions of (a) $LiCoO_2$, and (b) Al-LLZO, respectively.

Because the theoretical density of the two phases is similar (~5.1 g/cm^3), the volumetric and the gravimetric ratio are very close.

Because a thin Li_2CO_3 layer forms on the surface of the as-prepared composite pellets (see XPS and FIB-SEM in Fig. 3), pellets were polished before the application of current collectors and conductivity measurements.

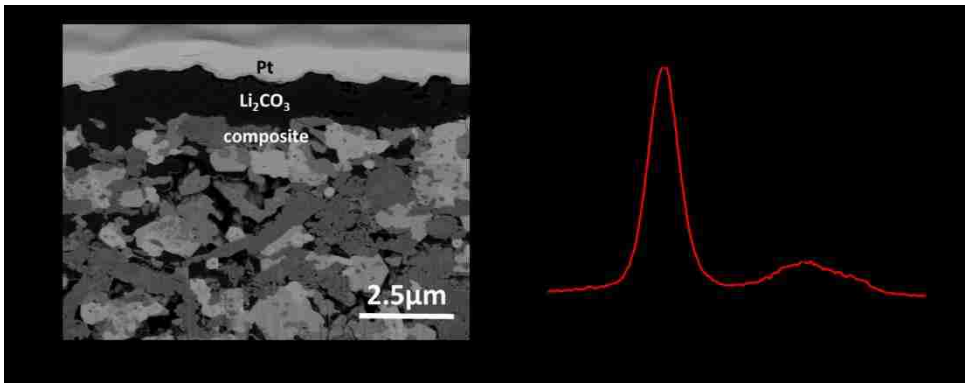

Fig. 3. (a) 2D slice image of air exposed sample, and (b) XPS of C 1s.

Fig. 4a shows the AC impedance spectrum of the $LiCoO_2$/Al-LLZO 1:1 composite sample measured in a symmetrical Au/composite/Au configuration. Because no low-frequency polarization process is observed, the electronic conduction is predominant.

A recent study[20] shows that when charge transfer between the two phases of a composite sample is negligible, the AC impedance spectrum does not include the parasitic resistance that originates from the ionic phase, and therefore the impedance at zero frequency is equal to the electronic resistance (Re) of the sample. This conclusion was further confirmed by the step-like behavior of the DC polarization/depolarization voltage curve (KEITHLEY 2400 SourceMeter) measured in an ion-blocking Au/Composite/Au configuration (Fig. 4b). Fig. 4b,c presents a well-defined linear ohmic behavior for the $LiCoO_2$/Al-LLZO 1:1 composite sample, suggesting that the conductivity is dominated by electron transport. $LiCoO_2$/Al-LLZO 3:1 and 1:3 samples also show similar behavior as that of 1:1 sample, as presented in Fig. S1 and S2. Resistance values derived from AC impedance spectra and the DC polarization/depolarization curves are very close and correspond to the electronic conductivity of 1.2×10^{-3}, 6.5×10^{-4}, and 2.2×10^{-5} S/cm for 3:1, 1:1, and 1:3 samples, respectively.

In order to derive the ionic conductivity of the composite samples, DC polarization measurements were performed using an electron-blocking cell.[21-23] Cell assembly and measurements were entirely performed inside an Argon filled glovebox. Fig. 4d shows the time dependent behavior of the polarization voltage for the $LiCoO_2$/Al-LLZO (1:1) sample. The potential gradually increases due to slow diffusion of lithium ions and eventually reaches a steady state value corresponding to ionic conductivity.[24] The chemical diffusion coefficient D_{Li^+} is extracted based on

$$D_{\mathrm{Li}^+} = \frac{L^2}{\pi^2 \tau^{\delta}}$$

and

$$U_{ion} = \frac{IL}{\sigma} + \frac{IL}{\sigma_{ion}}\frac{\sigma_{eon}}{\sigma}\left[1 - \frac{8}{\pi^2}\exp\left(-\frac{t}{\tau^{\delta}}\right)\right],$$

where I is the applied current, L the sample thickness, σ the total conductivity, and τ^{δ} the relaxation time.[25-28] Accordingly, a plot of $\ln|U(t)-U(t=\infty)|$ versus time is a straight line with a slope of τ^{δ} (Fig. 4d, inset).

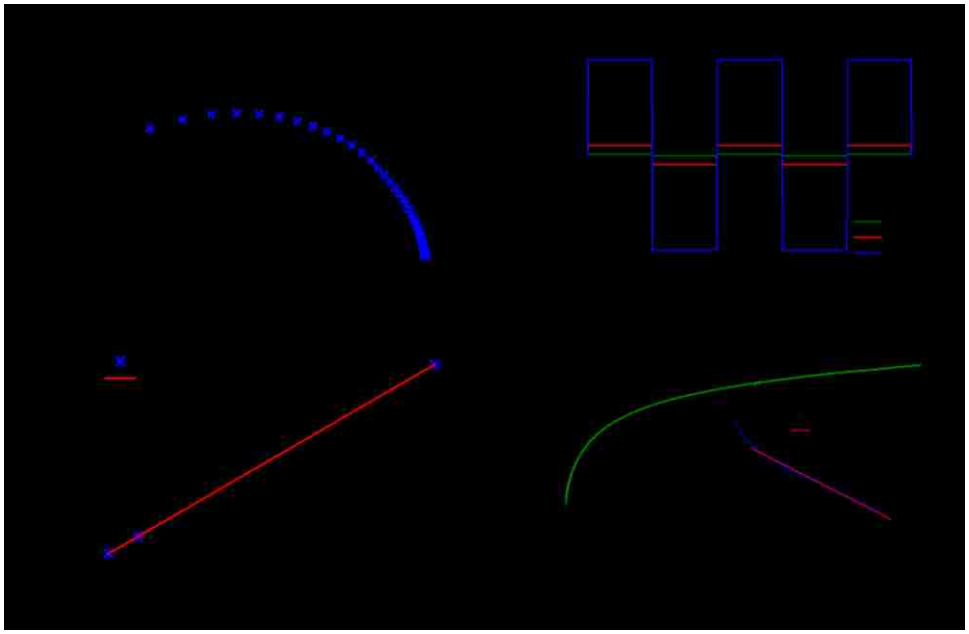

Fig. 4. (a) Impedance spectrum of $LiCoO_2$/Al-LLZO 1:1 composite sample, (b) DC polarization of the $LiCoO_2$/Al-LLZO 1:1 composite sample measured with Au/Composites/Au configuration, (c) *I-V* relationship extracted from (b), and (d) DC polarization measurement of $LiCoO_2$/Al-LLZO 1:1, and composite sample with LiAl/LiI/Composites/LiI/LiAl configuration.

Fig. 5 summarizes the electronic and ionic conductivities of the composite samples with varying amount of Al-LLZO, and shows regularities of the 1:3 and 3:1 composite samples. The $LiCoO_2$/Al-LLZO (3:1) sample exhibits an electronic conductivity of ~10^{-3} S/cm and decreases to 10^{-4} and 10^{-5} S/cm for the 1:1 and 1:3 samples, respectively. Ionic conductivity of all three composites, when compared to pure Al-LLZO pellet (~10^{-4} S/cm, see Fig. S3), is very low (~10^{-11} S/cm), and no obvious change is observed. On the basis of Fig. 5, the variation of electronic and ionic conductivities shows very different characteristics. Variation of electronic conductivity

indicates that electron conduction behavior is related to the ratio of electron conducting phase, and the changes are approximately linear. One the contrary, ionic conductivity was attenuated sharply in composites compared with sintered LLZO pellets, even in the composite sample with more than 75% of the Li-ion conducting LLZO phase.

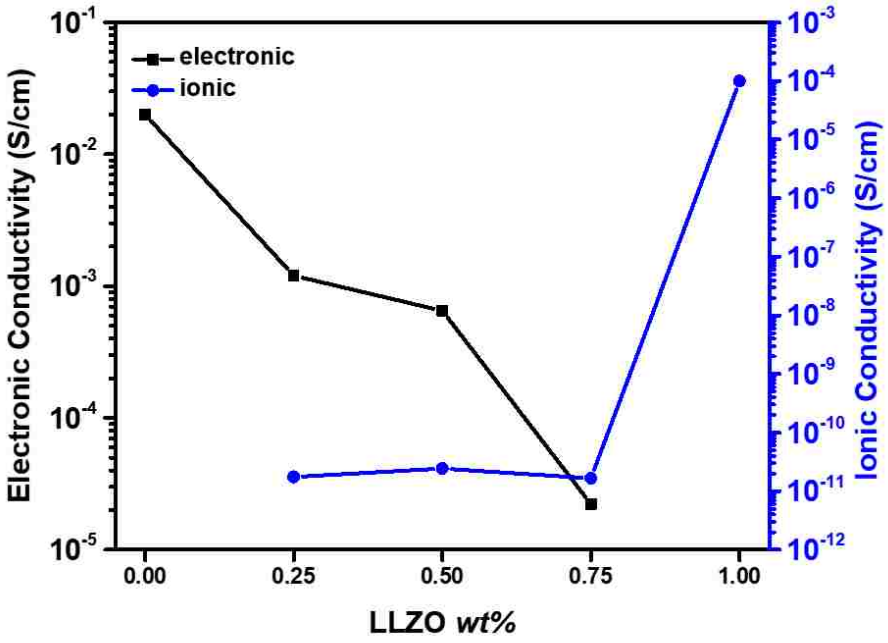

Fig. 5. Variation tendencies of electronic and ionic conductivities with the increasing amount of solid electrolyte. Electronic conductivity of $LiCoO_2$ is shown in Fig. S4.

2D and 3D reconstructed FIB-SEM images (Fig. 6) of $LiCoO_2$/Al-LLZO composites (1:1 weight ratio) were acquired from an FEI Helios NanoLab 660 DualBeam system using a gallium ion source. The light gray and dark gray particles in the BSE images correspond to Al-LLZO and $LiCoO_2$, respectively. The composite is not fully dense thus pores in black are observed (see SE images and EDS map in Fig. S5).

The 3D image of $LiCoO_2$/Al-LLZO composite was reconstructed from 280 2D slices (~30 nm for a single slice), as shown in Fig. 6b. Fig. 6a,b shows different

distributions of $LiCoO_2$ and Al-LLZO. Seemingly, Al-LLZO particles tend to agglomerate and form isolated areas, while $LiCoO_2$ forms a continuous network. This phenomenon could originate from their different surface energies. In particular $LiCoO_2$, in comparison with most oxides, exhibits a very low surface energy.[29] Overall, Al-LLZO particles/clusters form isolated regions surrounded by a continuous $LiCoO_2$ matrix. The distribution of Al-LLZO phase in composites (1:1 weight ratio) is presented in Fig. 6c, which is derived from Fig. 6b by the tuning grayness of the reconstructed 3D image. Fig. 6c further verifies that Al-LLZO is disconnected within the inspected volume.

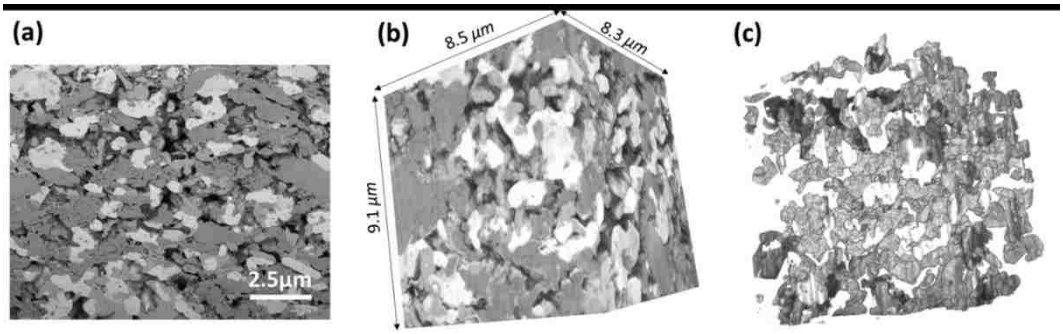

Fig. 6. (a) 2D slice of composites (1:1 ratio), (b) reconstructed 3D microstructures of composites, and (c) distribution of Al-LLZO phase in (b).

Fig. 7 provides additional evidence for the distribution of $LiCoO_2$ and Al-LLZO phases in the composite sample. We reconstructed a partial view of the 3D FIB-SEM image, with fixed xy and xz surfaces while the yz face is moving toward the x-axis. These images confirm that there is sufficient connectivity between the $LiCoO_2$ particles to pass electronic current, while the Al-LLZO particles form isolated regions that are ineffective in supporting charge-transfer and ion conduction.

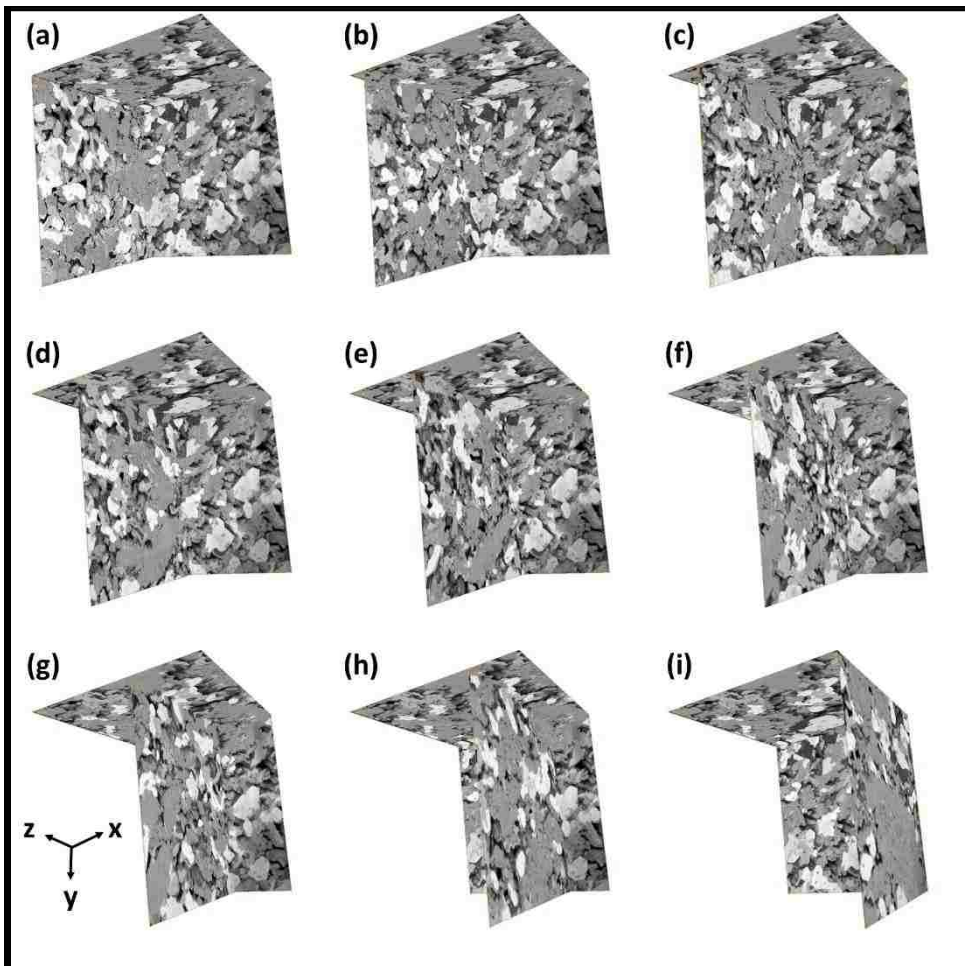

Fig. 7. Partial view of reconstructed 3D FIB-SEM.

Percolation theory has often been used in solid oxide fuel cells (SOFCs) to evaluate the effective conductivity of SOFC porous composite cathodes. On the basis of percolation theory of multiphase mixtures,[30] we assume that each particle, in a randomly packed mixture of particles, could belong to one of three types of clusters: Type (A), particles form a percolated cluster that extend throughout the entire thickness of the composite; Type (B), particles form a short network that is connected only to one side of the composite; Type (C), particles form a completely isolated cluster. Chen *et al.*[31] proposed that in a binary system the probability (P) of each particle i belonging to Type A clusters can be estimated by:

$$P_i = \left[1 - \left(\frac{3.764 - Z_{i,i}}{2}\right)^{2.5}\right]^{0.4},$$

where $Z_{i,i}$ is the number of contacts between an i particle and all of its neighboring i particles. They suggested that there is a threshold in the volume concentration of the particles below which the particles form only B and C clusters (P is 0 at $Z_{i,i} = \bar{Z}\frac{\psi_i^c/r_i}{\psi_i^c/r_i+\psi_e/r_e}$=1.764, $Z_{e,e} = \bar{Z}\frac{\psi_e^c/r_e}{\psi_e^c/r_e+\psi_i/r_i}$ =1.764). Above the percolation threshold, the composite still contains B and C clusters, but A clusters are the majority. This threshold depends on the volume fraction, radii, and average coordination number of the particles. A detailed analysis of composites with nonuniform distribution of particles is necessary to precisely predict the behavior of our samples. Above the percolation threshold, a very rough estimation of the effective electronic conductivity relative to the intrinsic conductivity of the pure phase can be expressed as

$$\sigma_{eff} = \sigma_{intrinsic}\left((1 - \Phi)\psi\mathrm{P}\right)^{\mu},$$

where the Bruggeman factor μ (the effects of tortuous conduction paths) is widely taken as 1.5 in composites.

It means that when sufficient percolation pathways are present, the electronic conductivity should be at least one or two magnitude lower than intrinsic conductivity. This is in good agreement with the measured electronic conductivity of our 1:1 composite sample (shown in Fig. 5), and therefore reasonable percolation pathways are obtained for the electron conducting component in this composite sample. This is also in agreement with the FIB-SEM images.

The ionic conductivity of the composite sample with 50% Al-LLZO phase is very low because of the presence of isolated areas of Al-LLZO and the absence of

percolation paths, meaning that Li-ions need to travel through poorly conducting Al-LLZO/$LiCoO_2$ interfaces and/or bulk $LiCoO_2$.

It should be noted that besides insufficient percolation, the presence of pores, blocking grain boundaries/interfaces,[32] and poor contact between the Al-LLZO particles could contribute to the poor ionic conductivity of the composite. It also implies that the effective conductivity equation might not be applicable to calculating ionic conductivity after taking these extra complexities into consideration.

Chapter 4 Conclusions

In summary, we have experimentally investigated the transport properties of an electronic-ionic composite. It shows that formation of percolation paths is necessary to achieve the expected ionic and electronic charge transport, and can be obtained by tuning the particle/pore size distribution and volume fraction of the components. However, the compositional characteristics of each phase, e.g., the surface energy of the particles and growth behavior at the annealing temperature may hinder access to the theoretically predicted percolation paths and the necessary connectivity between the particles. Therefore, improving the processing conditions of the composite cathodes in order to obtain uniform particle distribution is of pivotal importance. This study is the first step towards understanding electrical behavior of composites consisting of ion and electron conducting phases. It also hints that ion conduction behavior is more complicated than electron conduction behavior in electronic-ionic composites. Thus, we suggest the use of other Li-ion conducting compounds, such as amorphous sulfides or conducting polymers, to enhance the ion transport and therefore the utilization of composite cathodes for bulk-type all-solid-state batteries.

Chapter 5 Supplementary Information

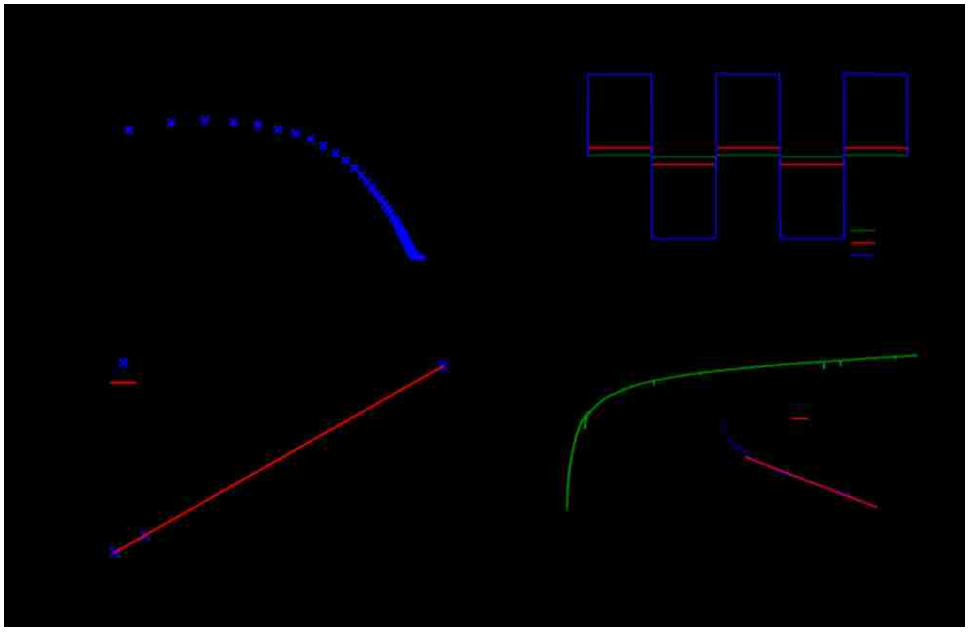

Fig. S1. (a) Impedance spectrum of $LiCoO_2$/Al-LLZO 3:1 composite sample, (b) DC polarization of the $LiCoO_2$/Al-LLZO 3:1 composite sample measured with Au/Composites/Au configuration, (c) I-V relationship extracted from (b), and (d) DC polarization measurement of $LiCoO_2$/Al-LLZO 3:1, and composite sample with LiAl/LiI/Composites/LiI/LiAl configuration.

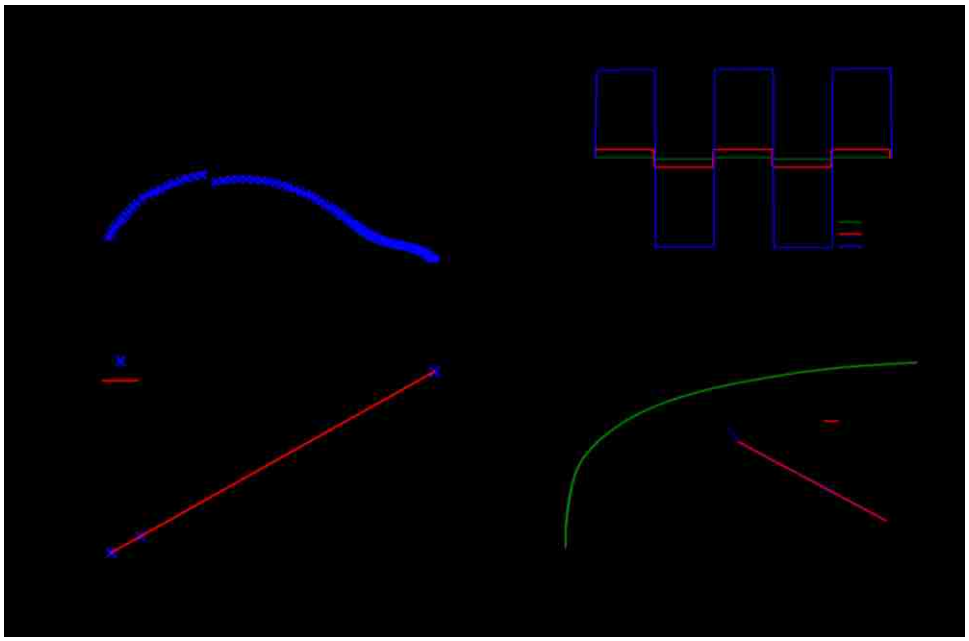

Fig. S2. (a) Impedance spectrum of $LiCoO_2$/Al-LLZO 1:3 composite sample, (b) DC polarization of the $LiCoO_2$/Al-LLZO 1:3 composite sample measured with Au/Composites/Au configuration, (c) I-V relationship extracted from (b), and (d) DC polarization measurement of $LiCoO_2$/Al-LLZO 1:3, and composite sample with LiAl/LiI/Composites/LiI/LiAl configuration.

Figure S3 shows the AC impedance spectrum of the Al-LLZO pellet sample measured in a symmetrical Au/composite/Au configuration using a Solartron 1260, at frequency range of 10^7-1 Hz, and AC amplitude of 50 mV. The fitting was performed using Zview software (Scribner Associates Inc.) to obtain the electrical properties. Bulk and grain boundary resistance values are 2057 Ω and 1357 Ω, respectively.

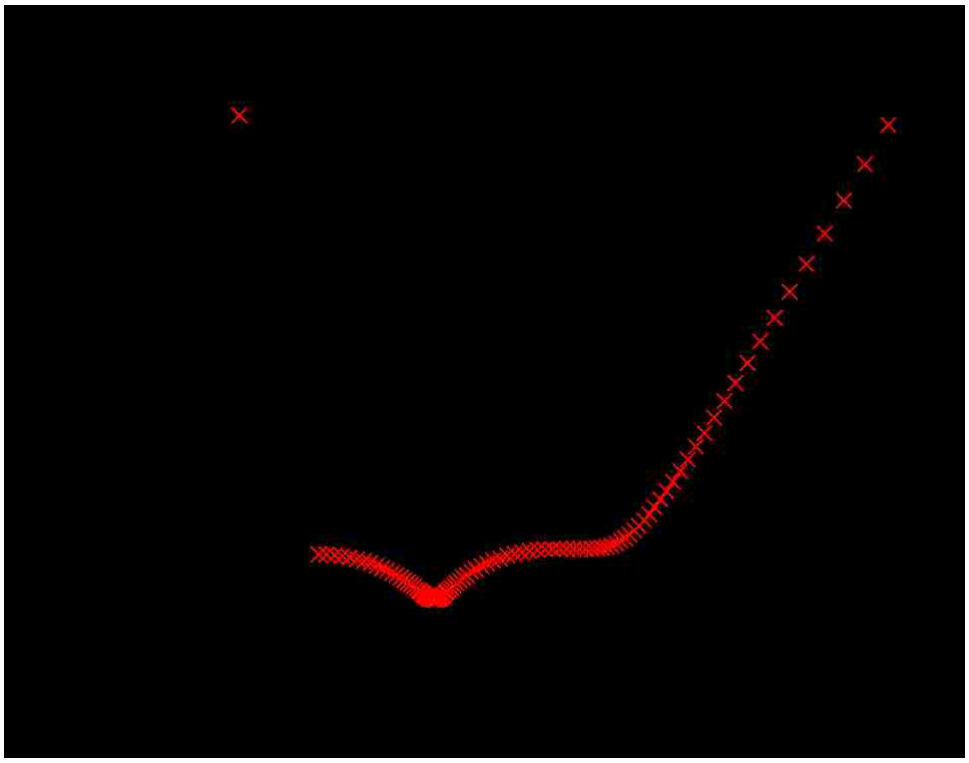

Fig. S3. (a) Impedance spectrum of Al-LLZO sintered pellet measured in air and at room temperature. Sample dimension: thickness 2.4 *mm*, diameter 8.2 *mm*.

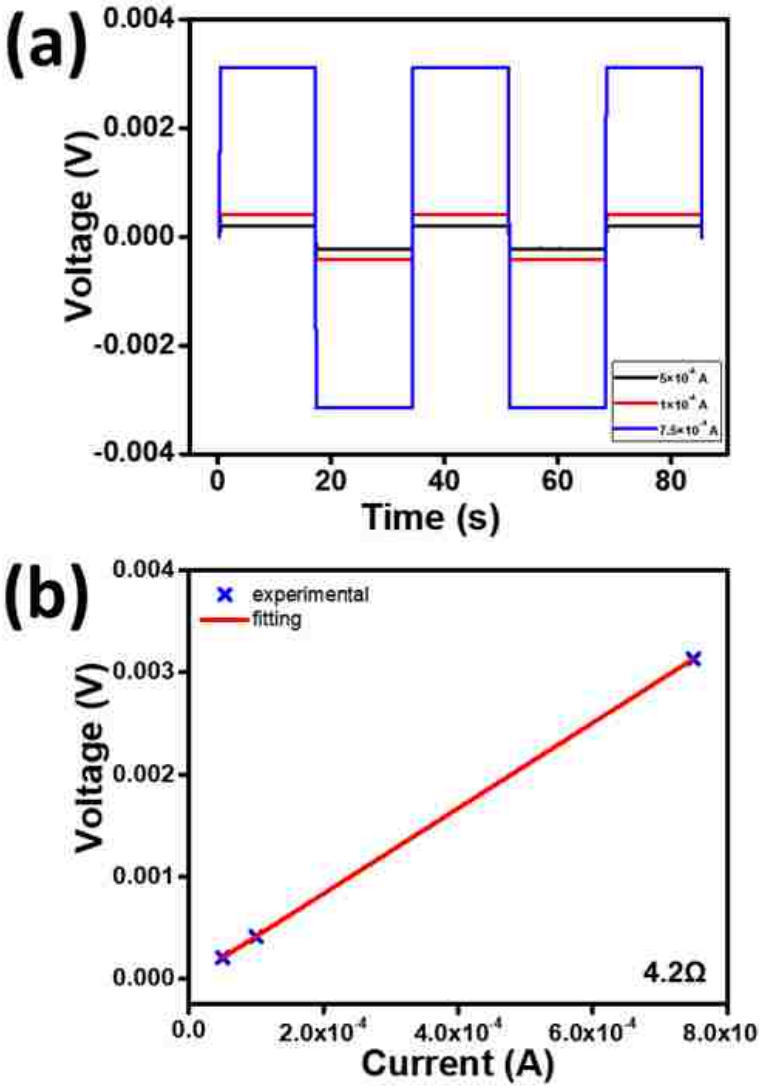

Fig. S4. (a) DC polarization measurement of the pure $LiCoO_2$ using the Au/Composites/Au configuration. (b) I-V relationship extracted from (a). Sample dimension: thickness 0.7 *mm*, diameter 10 *mm*.

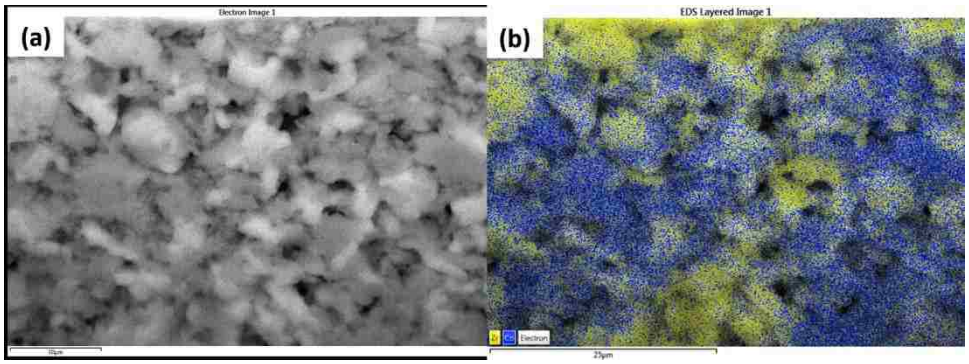

Fig. S5. (a) SEM image and (b) EDS map of LiCoO2/Al-LLZO 1:1 sample.

References

1. Kotobuki, M.; Munakata, H.; Kanamura, K.; Sato, Y.; Yoshida, T., Compatibility of $Li_7La_3Zr_2O_{12}$ solid electrolyte to all-solid-state battery using Li metal anode. *J. Electrochem. Soc.* 2010, *157* (10), A1076.
2. Chen, R.; Qu, W.; Guo, X.; Li, L.; Wu, F., The pursuit of solid-state electrolytes for lithium batteries: from comprehensive insight to emerging horizons. *Mater. Horiz.* 2016, *3* (6), 487-516.
3. Xia, W.; Xu, B.; Duan, H.; Guo, Y.; Kang, H.; Li, H.; Liu, H., Ionic conductivity and air stability of Al-doped $Li_7La_3Zr_2O_{12}$ sintered in alumina and Pt crucibles. *ACS Appl. Mater. Interfaces* 2016, *8* (8), 5335-42.
4. Jian, Z.; Hu, Y. S.; Ji, X.; Chen, W., NASICON-structured materials for energy storage. *Adv. Mater.* 2017, *29* (20), 1601925.
5. Manthiram, A.; Yu, X.; Wang, S., Lithium battery chemistries enabled by solid-state electrolytes. *Nat. Rev. Mater.* 2017, *2* (4), 16103.
6. Wu, J. F.; Pang, W. K.; Peterson, V. K.; Wei, L.; Guo, X., Garnet-type fast Li-ion conductors with high ionic conductivities for all-solid-state batteries. *ACS Appl. Mater. Interfaces* 2017, *9* (14), 12461-12468.
7. Zhang, J.; Zang, X.; Wen, H.; Dong, T.; Chai, J.; Li, Y.; Chen, B.; Zhao, J.; Dong, S.; Ma, J.; Yue, L.; Liu, Z.; Guo, X.; Cui, G.; Chen, L., High-voltage and free-standing poly(propylene carbonate)/$Li_{6.75}La_3Zr_{1.75}Ta_{0.25}O_{12}$composite solid electrolyte for wide temperature range and flexible solid lithium ion battery. *J. Mater. Chem. A* 2017, *5* (10), 4940-4948.
8. Han, F.; Zhu, Y.; He, X.; Mo, Y.; Wang, C., Electrochemical stability of $Li_{10}GeP_2S_{12}$ and $Li_7La_3Zr_2O_{12}$ solid electrolytes. *Adv. Energy Mater.* 2016, *6* (8), 1501590.
9. Kamaya, N.; Homma, K.; Yamakawa, Y.; Hirayama, M.; Kanno, R.; Yonemura, M.; Kamiyama, T.; Kato, Y.; Hama, S.; Kawamoto, K.; Mitsui, A., A lithium superionic conductor. *Nat Mater* 2011, *10* (9), 682-686.
10. Yan, Y.; Kühnel, R.-S.; Remhof, A.; Duchêne, L.; Reyes, E. C.; Rentsch, D.; Łodziana, Z.; Battaglia, C., A lithium amide-borohydride solid-state electrolyte with lithium-ion conductivities comparable to liquid electrolytes. *Adv. Energy Mater.* 2017, 1700294.
11. Buannic, L.; Orayech, B.; López Del Amo, J.-M.; Carrasco, J.; Katcho, N. A.; Aguesse, F.; Manalastas, W.; Zhang, W.; Kilner, J.; Llordés, A., Dual substitution strategy to enhance Li^+ ionic conductivity in $Li_7La_3Zr_2O_{12}$ solid electrolyte. *Chem. Mater.* 2017, *29* (4), 1769-1778.
12. Hansel, C.; Afyon, S.; Rupp, J. L., Investigating the all-solid-state batteries based on lithium garnets and a high potential cathode - $LiMn_{1.5}Ni_{0.5}O_4$. *Nanoscale* 2016, *8* (43), 18412-18420.
13. Orikasa, Y.; Gogyo, Y.; Yamashige, H.; Katayama, M.; Chen, K.; Mori, T.; Yamamoto, K.; Masese, T.; Inada, Y.; Ohta, T.; Siroma, Z.; Kato, S.; Kinoshita, H.; Arai, H.; Ogumi, Z.; Uchimoto, Y., Ionic conduction in lithium ion battery composite electrode governs cross-sectional reaction distribution. *Sci. Rep.* 2016, *6*, 26382.
14. Tao, X.; Liu, Y.; Liu, W.; Zhou, G.; Zhao, J.; Lin, D.; Zu, C.; Sheng, O.; Zhang, W.; Lee, H. W.; Cui, Y., Solid-state lithium-sulfur batteries operated at 37 °C with composites of nanostructured $Li_7La_3Zr_2O_{12}$/carbon foam and polymer. *Nano Lett.* 2017, *17* (5), 2967-2972.
15. Yan, X.; Li, Z.; Wen, Z.; Han, W., Li/$Li_7La_3Zr_2O_{12}$/$LiFePO_4$ all-solid-state battery with ultrathin nanoscale solid electrolyte. *J. Phys. Chem. C* 2017, *121* (3), 1431-1435.

16. Larson, A. C.; Von Dreele, R. B., Gsas. *General Structure Analysis System. LANSCE, MS-H805, Los Alamos, New Mexico* 1994.
17. Toby, B. H., EXPGUI, a graphical user interface for GSAS. *Journal of applied crystallography* 2001, *34* (2), 210-213.
18. Shin, D. O.; Oh, K.; Kim, K. M.; Park, K. Y.; Lee, B.; Lee, Y. G.; Kang, K., Synergistic multi-doping effects on the $Li_7La_3Zr_2O_{12}$ solid electrolyte for fast lithium ion conduction. *Sci. Rep.* 2015, *5*, 18053.
19. El-Shinawi, H.; Paterson, G. W.; MacLaren, D. A.; Cussen, E. J.; Corr, S. A., Low-temperature densification of Al-doped $Li_7La_3Zr_2O_{12}$: a reliable and controllable synthesis of fast-ion conducting garnets. *J. Mater. Chem. A* 2017, *5* (1), 319-329.
20. Siroma, Z.; Sato, T.; Takeuchi, T.; Nagai, R.; Ota, A.; Ioroi, T., AC impedance analysis of ionic and electronic conductivities in electrode mixture layers for an all-solid-state lithium-ion battery. *Journal of Power Sources* 2016, *316*, 215-223.
21. Amin, R.; Lin, C.; Peng, J.; Weichert, K.; Acartürk, T.; Starke, U.; Maier, J., Silicon-doped $LiFePO_4$ single crystals: growth, conductivity behavior, and diffusivity. *Adv. Funct. Mater.* 2009, *19* (11), 1697-1704.
22. Amin, R.; Balaya, P.; Maier, J., Anisotropy of Electronic and Ionic Transport in $LiFePO_4$ Single Crystals. *Electrochem. Solid-State Lett.* 2007, *10* (1), A13.
23. Amin, R.; Maier, J.; Balaya, P.; Chen, D. P.; Lin, C. T., Ionic and electronic transport in single crystalline $LiFePO_4$ grown by optical floating zone technique. *Solid State Ionics* 2008, *179* (27-32), 1683-1687.
24. Amin, R.; Lin, C.; Maier, J., Aluminium-doped $LiFePO_4$ single crystals. Part II. Ionic conductivity, diffusivity and defect model. *Phys. Chem. Chem. Phys.* 2008, *10* (24), 3524-9.
25. Amin, R.; Chiang, Y.-M., Characterization of electronic and ionic transport in $Li_{1-x}Ni_{0.33}Mn_{0.33}Co_{0.33}O_2$ (NMC333) and $Li_{1-x}Ni_{0.50}Mn_{0.20}Co_{0.30}O_2$ (NMC523) as a function of Li content. *J. Electrochem. Soc.* 2016, *163* (8), A1512-A1517.
26. Maier, J., *Physical chemistry of ionic materials: ions and electrons in solids*. John Wiley & Sons: 2004.
27. Yokota, I., On the theory of mixed conduction with special reference to conduction in silver sulfide group semiconductors. *J. Phys. Soc. Jpn.* 1961, *16* (11), 2213-2223.
28. Amin, R.; Balaya, P.; Maier, J., Anisotropy of electronic and ionic transport in $LiFePO_4$ single crystals. *Electrochem. Solid-State Lett.* 2007, *10* (1), A13-A16.
29. Maram, P. S.; Costa, G. C.; Navrotsky, A., Experimental confirmation of low surface energy in LiCoO(2) and implications for lithium battery electrodes. *Angew Chem Int Ed Engl* 2013, *52* (46), 12139-42.
30. Chen, D.; He, H.; Zhang, D.; Wang, H.; Ni, M., Percolation theory in solid oxide fuel cell composite electrodes with a mixed electronic and ionic conductor. *Energies* 2013, *6* (3), 1632-1656.
31. Chen, D.; Lin, Z.; Zhu, H.; Kee, R. J., Percolation theory to predict effective properties of solid oxide fuel-cell composite electrodes. *J. Power Sources* 2009, *191* (2), 240-252.
32. Gellert, M.; Gries, K. I.; Yada, C.; Rosciano, F.; Volz, K.; Roling, B., Grain boundaries in a lithium aluminum titanium phosphate-type fast lithium ion conducting glass ceramic: microstructure and nonlinear ion transport properties. *J. Phys. Chem. C* 2012, *116* (43), 22675-22678.

Vita

Education

2017.09	Master of Science: Materials Science and Engineering
	University of Kentucky – Lexington, Kentucky, the United States
2013.06	Master of Engineering: Physical Electronics
	Jinan University – Guangzhou, Guangdong, China
2010.06	Bachelor of Science: Applied Physics
	Jinan University – Guangzhou, Guangdong, China

Research Experience

University of Kentucky

Department of Chemical and Materials Engineering 08/2015-09/2017

- Garnet type solid electrolyte.
- Charge transport phenomenon in electronic-ionic composites.
- Symmetrical Li-ion all-solid-state battery.

Jinan University

Department of Physics 09/2010-06/2013

- Reduced Graphene Oxide (rGO).
- Catalytic performance of GO/rGO based nano-composites.
- Nano-zinc oxide (ZnO): growth, morphologies, and properties.
- Self-assembly patterned polystyrene (PS) nano-spheres.

Research Publications

1. Zhang, L.; Zhan, X.; Cheng, Y. T.; Shirpour, M. Charge Transport in Electronic–Ionic Composites. *The Journal of Physical Chemistry Letters* 2017, 8 (21), 5385-5389.
2. Zhang, L.; Du, L.; Yu, X.; Tan, S.; Cai, X.; Yang, P.; Gu, Y.; Mai, W., Significantly enhanced photocatalytic activities and charge separation mechanism of Pd-decorated ZnO–graphene oxide Nanocomposites. *ACS applied materials & interfaces* 2014, 6 (5), 3623-3629.
3. Zhang, L.; Du, L.; Cai, X.; Yu, X.; Zhang, D.; Liang, L.; Yang, P.; Xing, X.; Mai, W.; Tan, S., Role of graphene in great enhancement of photocatalytic activity of ZnO nanoparticle–graphene hybrids. *Physica E: Low-dimensional Systems and Nanostructures* 2013, 47, 279-284.
4. Xu, J.; Zhang, L.; Wang, Y.; Chen, T.; Al-Shroofy, M.; Cheng, Y. T., Unveiling the Critical Role of Polymeric Binders for Silicon Negative Electrodes in Lithium-Ion Full Cells. *ACS applied materials & interfaces* 2017, 9 (4), 3562-3569.
5. Mai, W.; Zhang, L.; Gu, Y.; Huang, S.; Zhang, Z.; Lao, C.; Yang, P.; Qiang, P.; Chen, Z., Mechanical and electrical characterization of semiconducting ZnO nanorings by direct nano-manipulation. *Applied Physics Letters* 2012, 101 (8), 081910.
6. Mai, W.; Liang, Z.; Zhang, L.; Yu, X.; Liu, P.; Zhu, H.; Cai, X.; Tan, S., Strain sensing mechanism of the fabricated ZnO nanowire-polymer composite strain sensors. *Chemical Physics Letters* 2012, 538, 99-101.
7. Chen, T.; Hu, J.; Zhang, L.; Pan, J.; Liu, Y.; Cheng, Y.-T. High performance binder-free SiOx/C

composite LIB electrode made of SiOx and lignin. *Journal of Power Sources* 2017, 362 (Supplement C), 236-242.
8. Yang, P.; Wang, K.; Liang, Z.; Mai, W.; Wang, C.-x.; Xie, W.; Liu, P.; Zhang, L.; Cai, X.; Tan, S.; Song, J. Enhanced wettability performance of ultrathin ZnO nanotubes by coupling morphology and size effects. *Nanoscale* 2012, 4 (18), 5755-5760.
9. Liang, Z.; Cai, X.; Tan, S.; Yang, P.; Zhang, L.; Yu, X.; Chen, K.; Zhu, H.; Liu, P.; Mai, W. Fabrication of n-type ZnO nanowire/graphene/p-type silicon hybrid structures and electrical properties of heterojunctions. *Physical Chemistry Chemical Physics* 2012, 14 (46), 16111-16114.
10. Liang, Z.; Cui, H.; Wang, K.; Yang, P.; Zhang, L.; Mai, W.; Wang, C.-X.; Liu, P. Morphology-controllable ZnO nanotubes and nanowires: synthesis, growth mechanism and hydrophobic property. *CrystEngComm* 2012, 14 (5), 1723-1728.